Remote electrochemical modulation of pK_a in a rotaxane by co-conformational allostery

Giulio Ragazzon,[a] Christian Schäfer,[a] Paola Franchi,[a] Serena Silvi,[a] Benoit Colasson,[a,b] Marco Lucarini*[a] and Alberto Credi*[c,d]

[a] Dipartimento di Chimica "G. Ciamician", Università di Bologna, via Selmi 2, 40126 Bologna, Italy

[b] Laboratoire de Chimie et de Biochimie Pharmacologiques et Toxicologiques (CNRS UMR 8601), Université Paris Descartes Sorbonne Paris Cité, 45 rue des Saints-Pères, 75006 Paris, France

[c] Dipartimento di Scienze e Tecnologie Agro-alimentari, Università di Bologna, viale Fanin 50, 40127 Bologna, Italy

[d] CLAN – Center for Light Activated Nanostructures, Università di Bologna and Consiglio Nazionale delle Ricerche, via Gobetti 101, 40129 Bologna, Italy

SUPPORTING INFORMATION

1. Experimental procedures

Materials and methods. Spectroscopic grade (Uvasol) acetonitrile was purchased from Merck; ferrocene (Fc) and triflic acid (TrH) were purchased from Aldrich; tetraetylammonium hexafluorophosphate ($TEAPF_6$), tetrabutylammonium hexafluorophosphate ($TBAPF_6$) and phosphazene base N-*t*-butyl-N′,N′,N″,N″,N‴,N‴-hexamethylphosphorimidic triamide (P_1-*t*-Bu) were purchased from Fluka. All chemicals were used as received, without further purification. P_1-*t*-Bu and TrH were added in the electrochemical cell or in the cuvette from a concentrated acetonitrile solution (typically 40 or 4 mM).

Electrochemical measurements. Cyclic voltammetric (CV) experiments were carried out at room temperature in argon-purged acetonitrile or acetone (Uvasol) with an Autolab 30 multipurpose instrument interfaced to a PC. The working electrode was a glassy carbon electrode (Amel; 0.07 cm^2); its surface was routinely polished with a 0.3 μm alumina-water slurry on a felt surface. The counter electrode was a Pt wire, separated from the solution by a frit; an Ag wire was employed as a quasi-reference electrode, and ferrocene (Fc) was present as an internal standard [$E_{1/2}(Fc^+/Fc)$ = +0.395 V vs SCE]. Ferrocene was added from a concentrated acetonitrile solution (typically 0.1 M). The concentration of the compounds examined was 4×10^{-4} M; tetraetylammonium hexafluorophosphate ($TEAPF_6$) 0.04 M was added as supporting electrolyte. The IR compensation implemented within the Autolab 30 was used, and every effort was made throughout the experiments to minimize the resistance of the solution. In any instance, the full electrochemical reversibility of the voltammetric wave of ferrocene was taken as an indicator of the absence of uncompensated resistance effects. Differential pulse voltammograms (DPV) were performed with a scan rate of 20 mV s^{-1}, a pulse height of 75 mV, and a duration of 40 ms. For reversible processes the halfwave potential values were obtained from the DPV peaks and from an average of the cathodic and anodic cyclic voltammetric peaks. The potential values for chemically irreversible processes were estimated from the DPV peaks.

Experimental errors. The error on pK_a values is estimated to be ±0.2 units, corresponding to ΔE = ±1 kJ mol^{-1}. This error is calculated as the average mean square root for the difference in the pK_a value reported for four bases investigated both in refs. S1 and S2. The experimental error on the potential values is ±0.01 V, corresponding to ΔE = ±1 kJ/mol^{-1}. The experimental error on the equilibrium constant K = 1.5 determined by CV titrations (Figs. S9-S10) is estimated to be ΔK = ±0.3, corresponding to ΔE = ±1 kJ mol^{-1}. The experimental error on the energy values reported in Fig. 5 is estimated to be ±2 kJ/mol, as in most cases they derive from the difference of two energy values.

2. Electrochemical data

Table S1. Reduction potential values for the studied compounds. Argon purged $CH_3CN/TEAPF_6$, all values in V vs SCE.

	Compound	$bpy^{2+}\rightarrow bpy^{(+\bullet)}$	$bpy^{2+}\rightarrow bpy^{(+\bullet)}$	$bpy^{(+\bullet)}\rightarrow bpy^{(0)}$	$bpy^{(+\bullet)}\rightarrow bpy^{(0)}$
		CV	DPV	CV	DPV
2H^{3+}	Axle component	–0.335	–0.34(0)	–0.765	–0.77(1)
	+ TBA 1 eq	–0.353	–0.35(8)	–0.789	–0.78(8)
	+ TBA 22.8 eq	–0.359	–0.3(6)	–0.795	–0.79(3)
	+ TBA 22.8 eq + TrH	–0.336	–0.33(7)	–0.753	–0.75(6)
	+ P_1-*t*-Bu 1 eq	–0.352	–0.35(8)	–0.787	–0.79(0)
	+ P_1-*t*-Bu 1 eq + TrH	–0.329	–0.33(5)	–0.744	–0.74(6)
1H^{3+}	Rotaxane	–0.334	–0.34(0)	–0.764	–0.76(5)
	+ TBA 22.8 eq	irreversible	–0.52(8)	–0.773	–0.77(0)
	+ TBA 22.8 eq + TrH	–0.336	–0.34(1)	–0.763	–0.76(3)
	+ P_1-*t*-Bu 1 eq	–0.562	–0.57(0)	–0.957	–0.96(0)
	+ P_1-*t*-Bu 1 eq + TrH	–0.331	–0.33(5)	–0.672	–0.76(2)

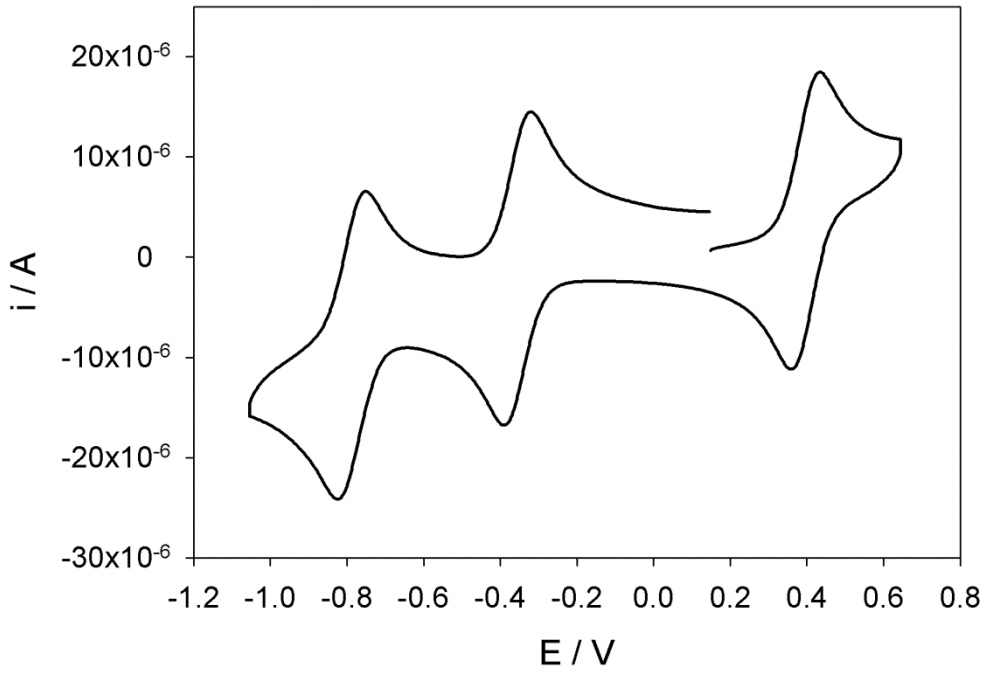

Fig. S1. Cyclic voltammetric pattern of the axle **2**H^{3+} upon addition of 1 equivalent of TBA. The process at +0.395 V vs SCE is due to the ferrocene used as an internal standard. Scan rate 300 mV s^{-1}.

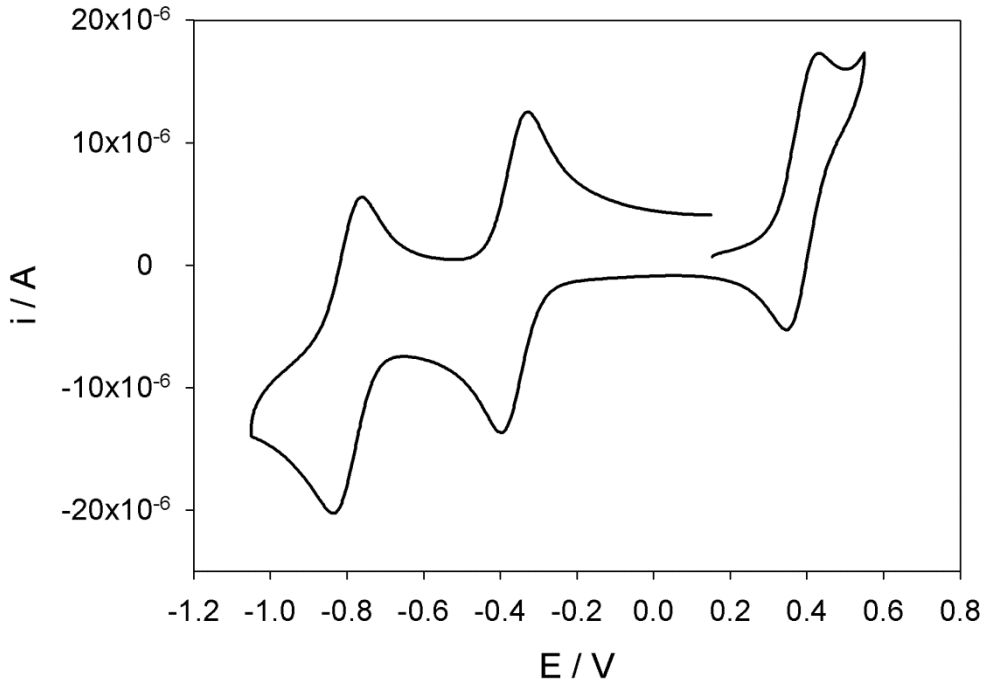

Fig. S2. Cyclic voltammetric pattern of the axle **2**H^{3+} upon addition of 22.8 equivalents of TBA. Scan rate 300 mV s^{-1}.

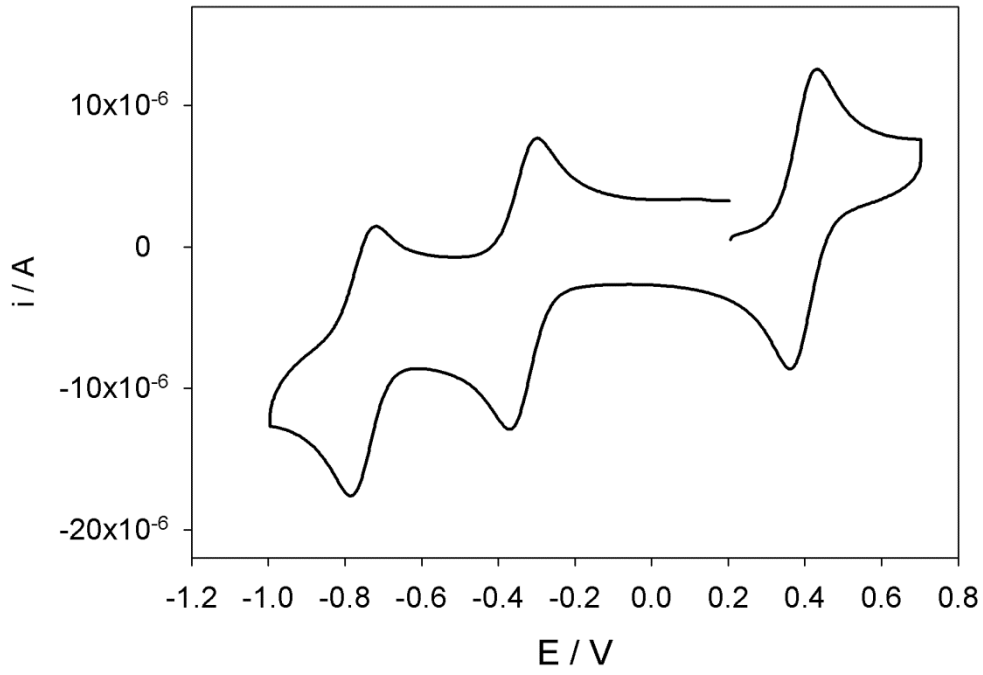

Fig. S3. Cyclic voltammetric pattern of the axle **2**H^{3+} upon addition of 22.8 equivalents of TBA and 22.8 equivalents of triflic acid. Scan rate 300 mV s^{-1}.

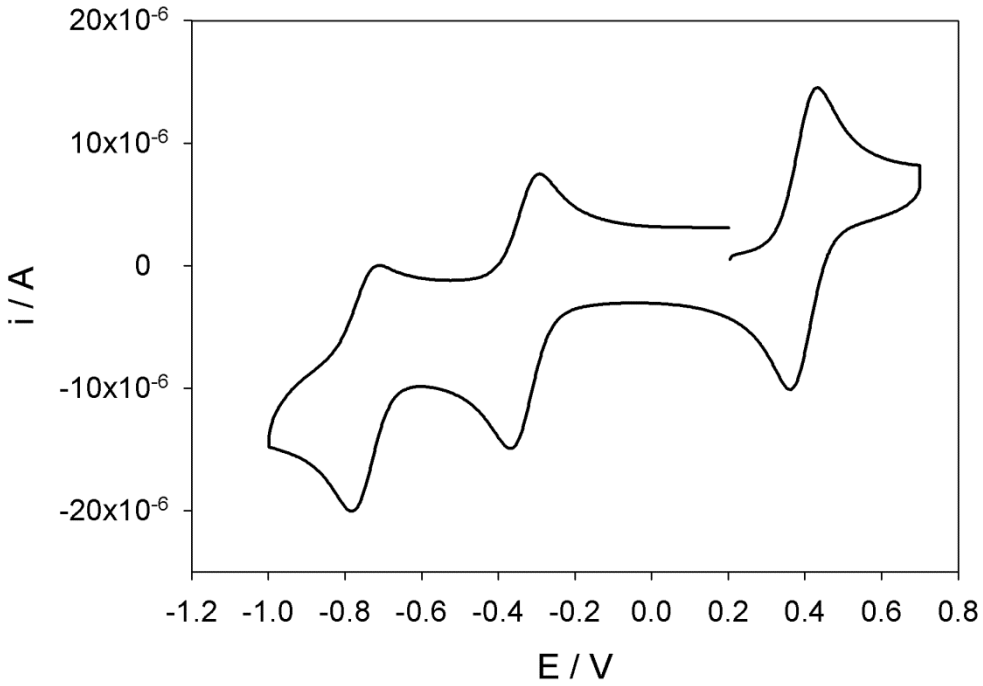

Fig. S4. Cyclic voltammetric pattern of the axle **2**H^{3+} upon sequential addition of 1 equivalent of phosphazene base and 1 equivalent of triflic acid. Scan rate 300 mV s^{-1}.

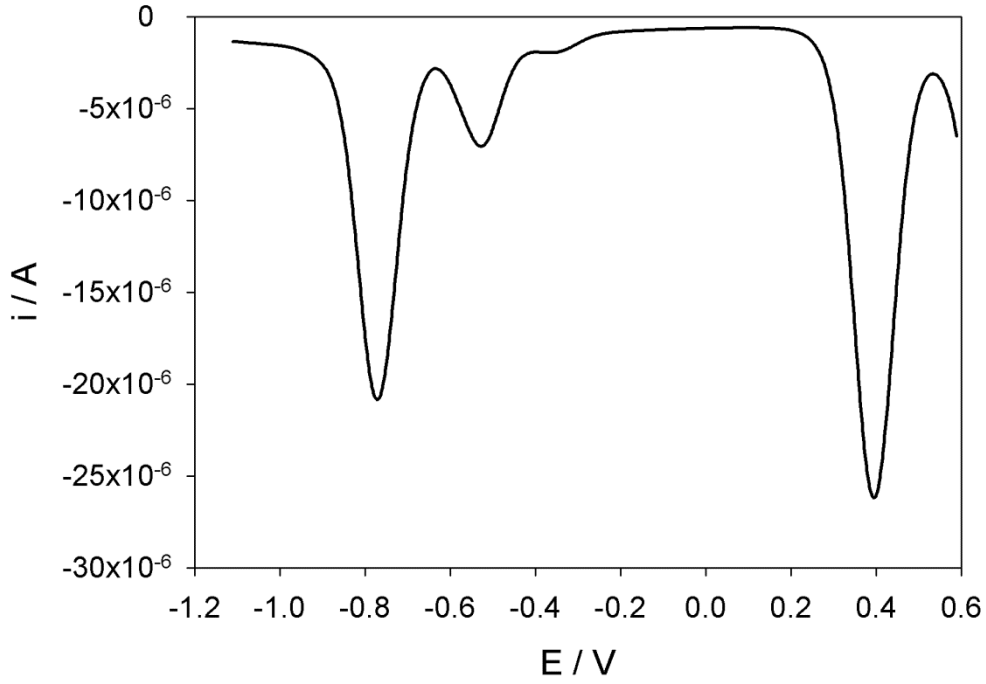

Fig. S5. Differential pulse voltammetric pattern of the rotaxane **1**H^{3+} upon addition of 22.8 equivalents of TBA.

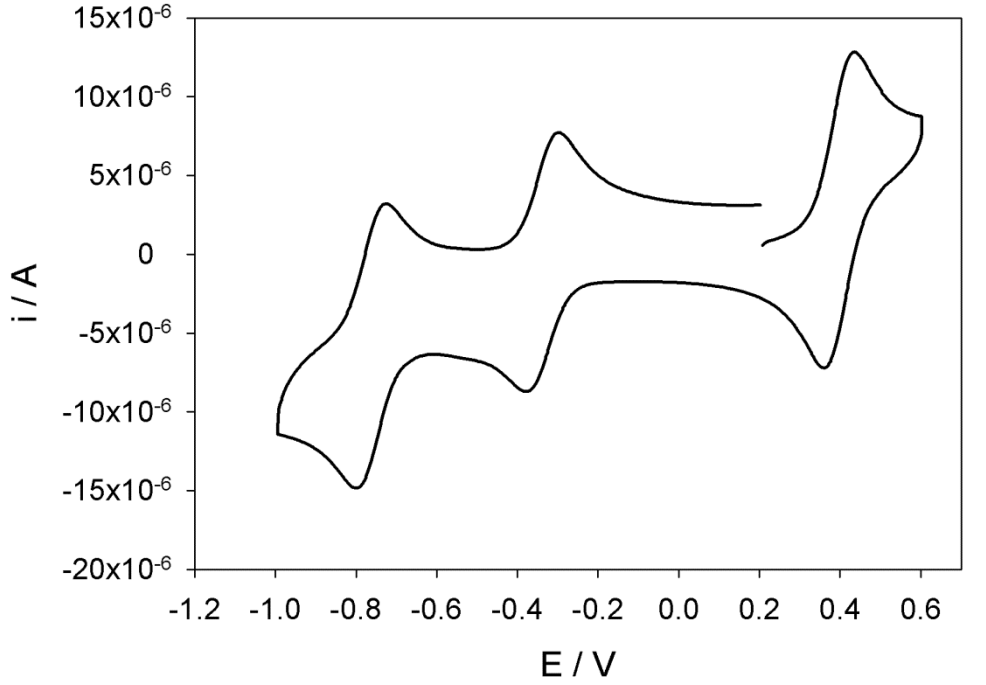

Fig. S6. Cyclic voltammetric pattern of the rotaxane **1**H^{3+} upon sequential addition of 22.8 equivalents of TBA and 22.8 equivalents of triflic acid. Scan rate 300 mV s^{-1}.

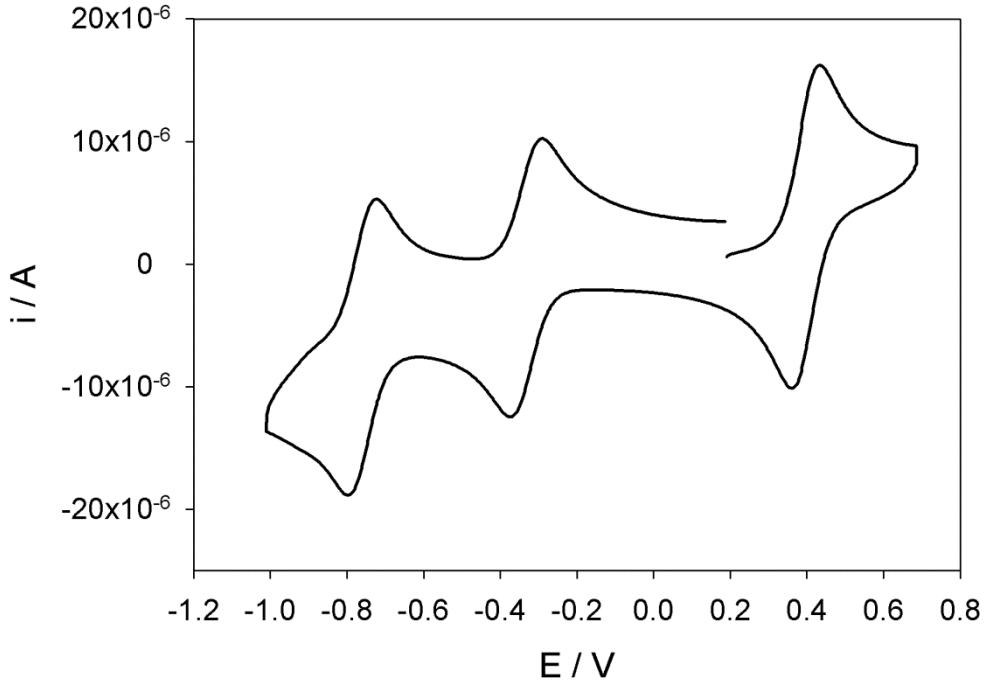

Fig. S7. Cyclic voltammetric pattern of the rotaxane **1**H^{3+} upon sequential addition of 1 equivalent of phosphazene base and 1 equivalent of triflic acid. Scan rate 300 mV s^{-1}.

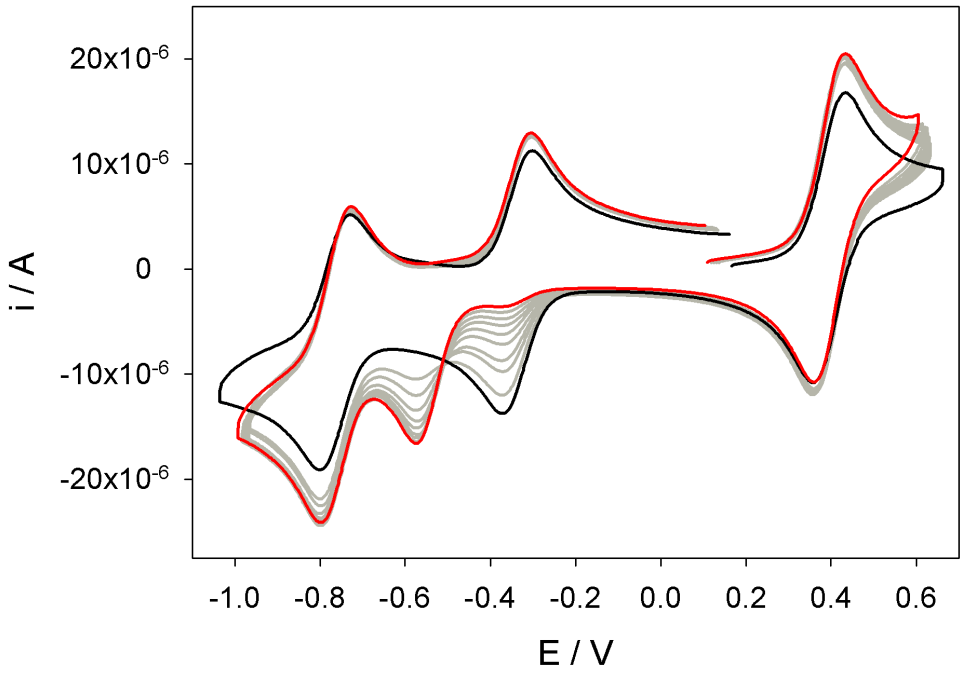

Fig. S8. Cyclic voltammetric pattern of the rotaxane **1**H^{3+} (black) upon addition of increasing amounts of TBA up to 22.8 equivalents (red). Scan rate 300 mV s^{-1}.

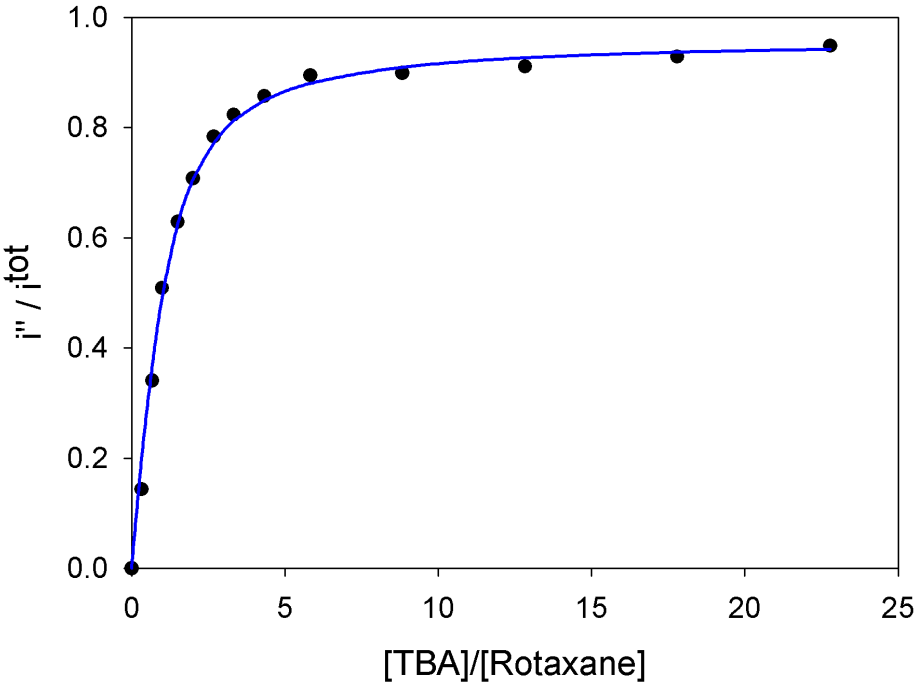

Fig. S9. Relative intensity of the current related to the reduction of the bipyridinium unit surrounded by the macrocycle, with respect to the total current relative to the first reduction process (only the anodic current is considered), at increasing amounts of added TBA base (black dots; voltammetric curves shown in Fig. S8). The equilibrium constant of the deprotonation reaction, obtained by data fitting (blue line) is K = 1.5.

3. EPR Spectra

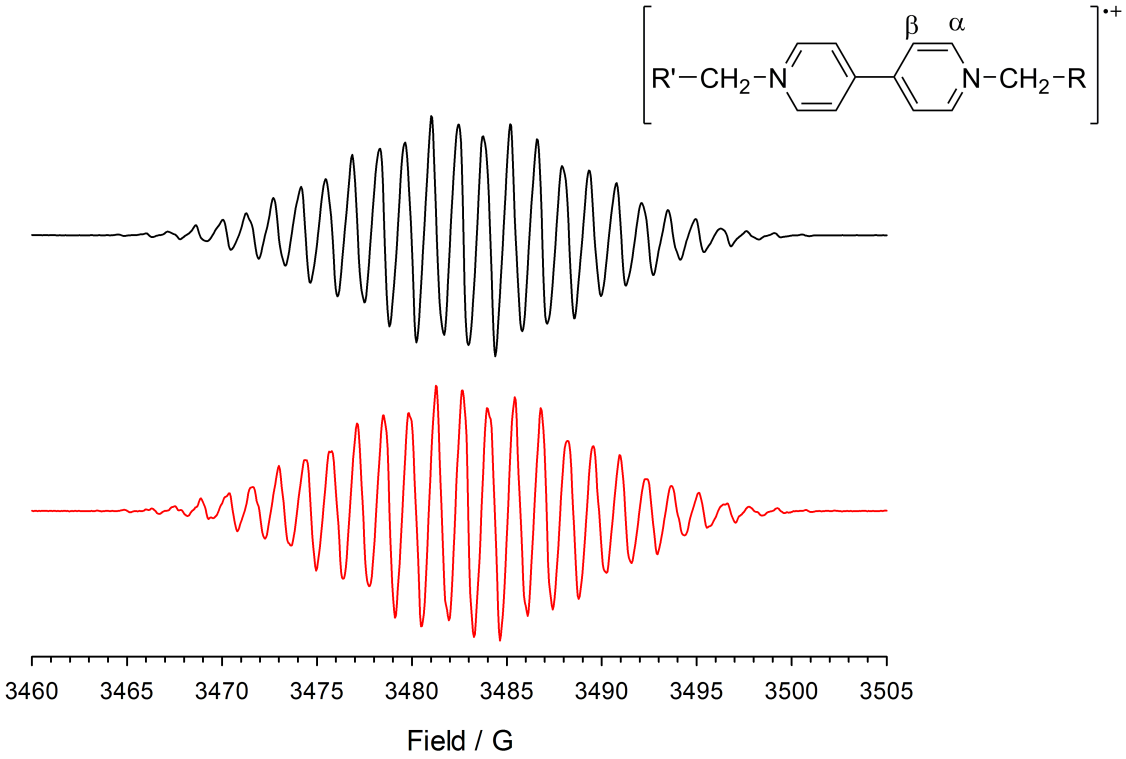

Fig. S10. EPR spectra of the radical cation derived from the free axle before (black trace) and after addition of 1 equivalent of P_1-*t*-Bu (red trace). Conditions: N_2 purged $CH_3CN/TBAPF_6$, room temperature.

4. Energy-level diagram

This section illustrates the reasoning and the calculations performed to obtain the simplified energy-level diagram shown in Fig. 5. The bottom reasoning is that the redox-induced pK_a change is associated to a destabilization of the apparent conjugate base $\mathbf{1}^{(n+)}$(M⊃bpy$^{(n+)}$), *n* = 0, 1 or 2, upon reduction of the bpy site (Fig. 5, right). Moreover, as the reduction process does not affect significantly the ammonium-macrocycle interaction in the corresponding conjugated acids $\mathbf{1}H^{+(n+)}$(M⊃amH$^+$), these species can be taken as reference in each redox state (Fig. 5, left). It is thus possible to predict the behavior of the system upon addition of P_1-*t*-Bu instead of TBA, because the associated free energy change can be fully ascribed to a destabilization of the reference states, in which the rotaxane is protonated and the added base is deprotonated (Fig. 5, left). The energy

difference reflects the cost of having P_1-*t*-Bu deprotonated instead of TBA, and is quantified by the difference in pK_a between their conjugated acids, P_1-*t*-BuH^+ and TBAH^+.

More in detail, as discussed in the text, relative free energy changes are considered in order to compare at a glance the behavior of the system in the presence of different bases and in different redox states. Fig. S11, panel A, shows all the energy levels available to the ensemble [**1**$H^{+(n+)}$ + **B**], where **B** = TBA or P_1-*t*-Bu, and *n* = 0, 1 or 2. The italicized numbers (*1,2*) denote the different bases and the letters (*a*,*b*,*c*; α,β,γ) denote the different redox states.

As the presence of M on the amH^+ site does not affect the redox behavior of the bipyridinium site, the energy differences *1b*–*1a* (or *2b*–*2a*) and *1c*–*1b* (or *2c*–*2b*) are related to the first and second reduction potentials of bpy^{2+}, respectively, in the protonated rotaxane (**1**H^{3+}) or in the free axle (**2**H^{3+}). The energy differences 1β–1α and 1γ–1β are related to the first and second reduction potentials of bpy^{2+}, respectively, in the deprotonated rotaxane (**1**$^{2+}$), in which the bpy unit is surrounded by the ring. Such differences are equal to 2β–2α and 2γ–2β, respectively, because the inherent redox properties of **1**$^{2+}$ do not depend on the base used to deprotonate **1**H^{3+}. The energy differences 1α–*1a*, 1β–*1b*, and 1γ–*1c* are determined by the basic strength of TBA (i.e., the pK_a of TBAH^+) and the acid strength of the rotaxane (i.e., its pK_a) in the dicationic, radical cationic and neutral states, respectively. Similarly, the energy differences 2α–*2a*, 2β–*2b*, and 2γ–*2c* are determined by the basic strength of P_1-*t*-Bu (i.e., the pK_a of P_1-*t*-BuH^+) and the acid strength of the rotaxane (i.e., its pK_a) in the dicationic, radical cationic and neutral states, respectively.

The full diagram shown in Fig. S11, panel A, can be simplified according to the two following remarks:

1) As noted above, the inherent redox properties of the deprotonated rotaxane (that determine the energy differences β–α and γ–β) do not depend on the base used to generate it. Thus, one can shift the levels so that the energies of the corresponding conjugated acids, TBAH^+ and P_1-*t*-BuH^+, are matched. As the energy differences 1β–1α and 1γ–1β are equal to 2β–2α and 2γ–2β, respectively, levels 1α and 2α, 1β and 2β, and 1γ and 2γ, merge to yield states α (*n* = 2), β (*n* = 1) and γ (*n* = 0) (Fig. S11, panel B, right). In this way, the energy gap *2a*–*1a* (or *2b*–*1b* and *2c*–*1c*) is directly related to the difference in the basic strength of the two bases (i.e., the difference in the pK_a values of TBAH^+ and P_1-*t*-BuH^+).

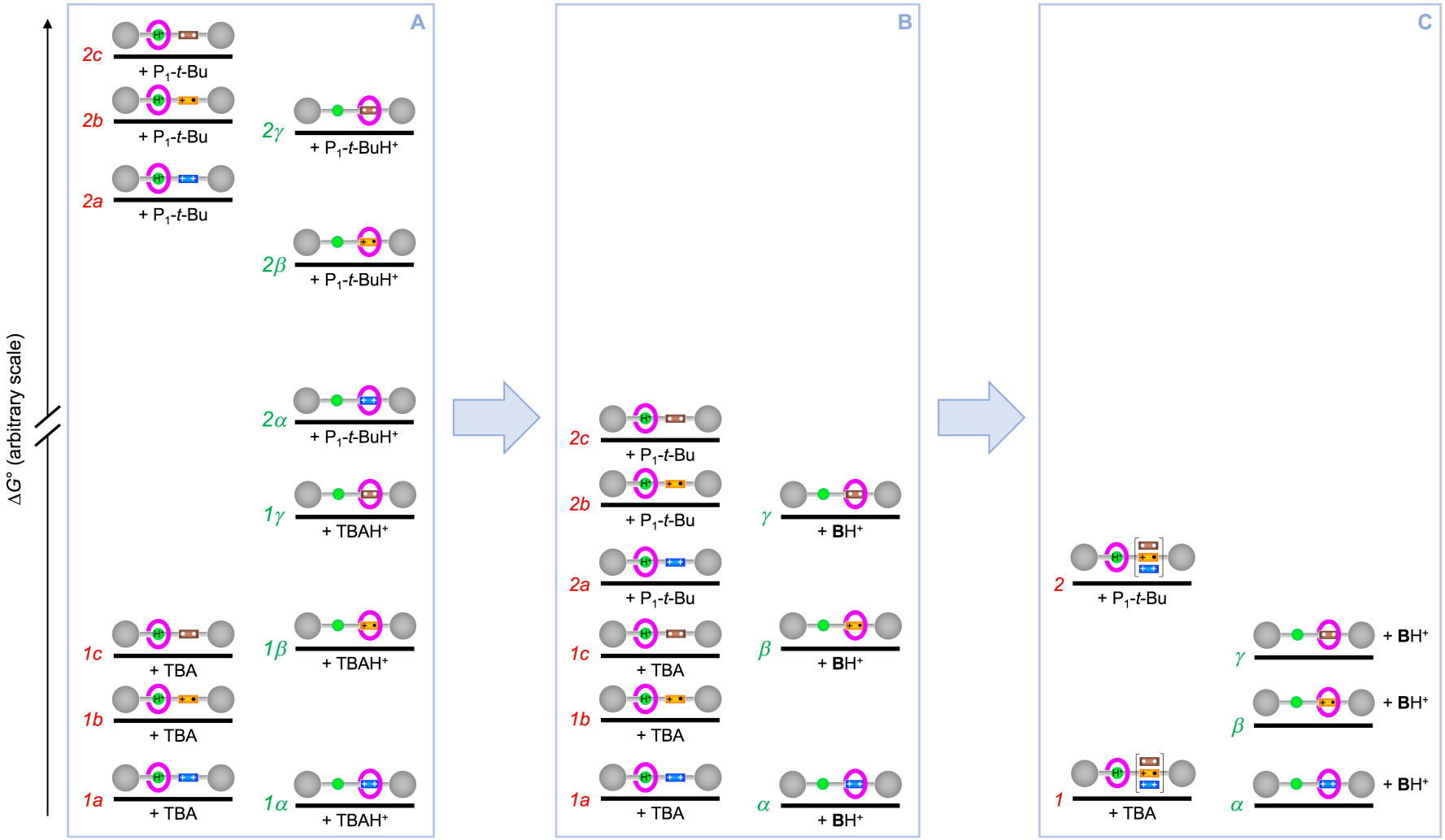

Fig. S11. (A) Energy levels available to the ensemble [**1**H$^{+(n+)}$ + **B**], where **B** = TBA or P$_1$-*t*-Bu and *n* = 0, 1 or 2. (B) Diagram in which the levels in (A) are shifted to align the energies of deprotonated rotaxanes **1**$^{(n+)}$ (*n* = 0, 1 or 2) in the same oxidation state, obtained with different bases. (C) Diagram in which the levels in (B) are shifted to align the energies of protonated rotaxanes **1**H$^{+(n+)}$ (*n* = 0, 1 or 2) in different oxidation states, in the presence of the same base.

2) The redox state of bpy has a negligible influence on the strength of the M⊃amH$^+$ interaction (vide supra). Thus, one can shift the levels to match the energies of protonated rotaxanes in different oxidation states in the presence of the same base. As the energy differences *2a*–*1a*, *2b*–*1b* and *2c*–*1c* are equal, levels *1a*, *1b* and *1c* merge to yield state *1*, which represents the protonated rotaxane (irrespective of its oxidation state) in the presence of TBA, and levels *2a*, *2b* and *2c* merge to yield state *2*, which represents the protonated rotaxane (irrespective of its oxidation state) in the presence of P_1-*t*-Bu. Notably, levels α, β and γ do not match because the M⊃bpy$^{(n+)}$ interaction does depend on the oxidation state of bpy.

The simplified diagram shown in Fig. S11, panel C (and Fig. 5), provides a compact representation of the main results presented in this study. In fact, as noted above, the energy difference *2*–*1* can be determined from the difference of pK_a of P_1-*t*-BuH$^+$ and TBAH$^+$, and enables a quick comparison of the strength of the bases that react with the rotaxane. The energy differences β–α and γ–β are the changes in the charge-transfer interaction between M and bpy on going from bpy^{2+} to bpy$^{(+\bullet)}$, and from bpy$^{(+\bullet)}$ to bpy$^{(0)}$, respectively. These values, which obviously do not depend on the strength of the base used to deprotonate the rotaxane, can be determined from the redox potential values as discussed in the following. Another known quantity is the energy difference between levels *1* and α, measured from the titration of **1**H^{3+} with TBA (Fig. S9).

The energy difference between the charge-transfer interactions in M⊃bpy$^{(+\bullet)}$ and M⊃bpy^{2+} (energy difference β–α in Fig. S11C) was estimated from the thermodynamic square cycle represented in Fig. S12, involving rotaxane **1**H^{3+}, the P_1-*t*-Bu base, and one-electron reduction/oxidation processes.

The reaction on the left is the reduction of bpy^{2+} to bpy$^{(+\bullet)}$ in the **1**H^{3+}(M⊃amH$^+$) rotaxane in the presence of P_1-*t*-Bu (before any acid-base reaction occurs), and we take its associated redox potential as that of **1**H^{3+} alone ($E_{1/2}$ = –0.34 V *vs* SCE, Table S1). The reaction on the right is the bpy^{2+}→bpy$^{(+\bullet)}$ reduction in the **1**$^{2+}$(M⊃bpy^{2+}) rotaxane in the presence of P_1-*t*-BuH$^+$; the deprotonated rotaxane is obtained upon reaction of **1**H^{3+} with P_1-*t*-Bu, and its redox potential can be measured ($E_{1/2}$ = –0.57 V *vs* SCE, Table S1). In the reasonable approximation that standard redox potentials ($E°$) correspond to halfwave potentials ($E_{½}$), the $\Delta G°$ values of the redox reactions can be calculated from CV data (equations S1-S2; *z*

= 1 is the number of exchanged electrons, F is Faraday's constant, $E_{½,free}$ and $E_{½,compl}$ are, respectively, the halfwave potential values for the bpy^{2+} unit free and complexed by M):

$$\Delta G_2^\circ = -\,z\,F\,E^\circ_{compl} \cong -\,z\,F\,E_{½,compl} = -\,1 \times 96480 \times (-0.57) = 55.0 \text{ kJ mol}^{-1} \qquad \text{(S1)}$$

$$\Delta G_4^\circ = -\,z\,F\,E^\circ_{free} \cong -\,z\,F\,E_{½,free} = -\,1 \times 96480 \times (-0.34) = 32.8 \text{ kJ mol}^{-1} \qquad \text{(S2)}$$

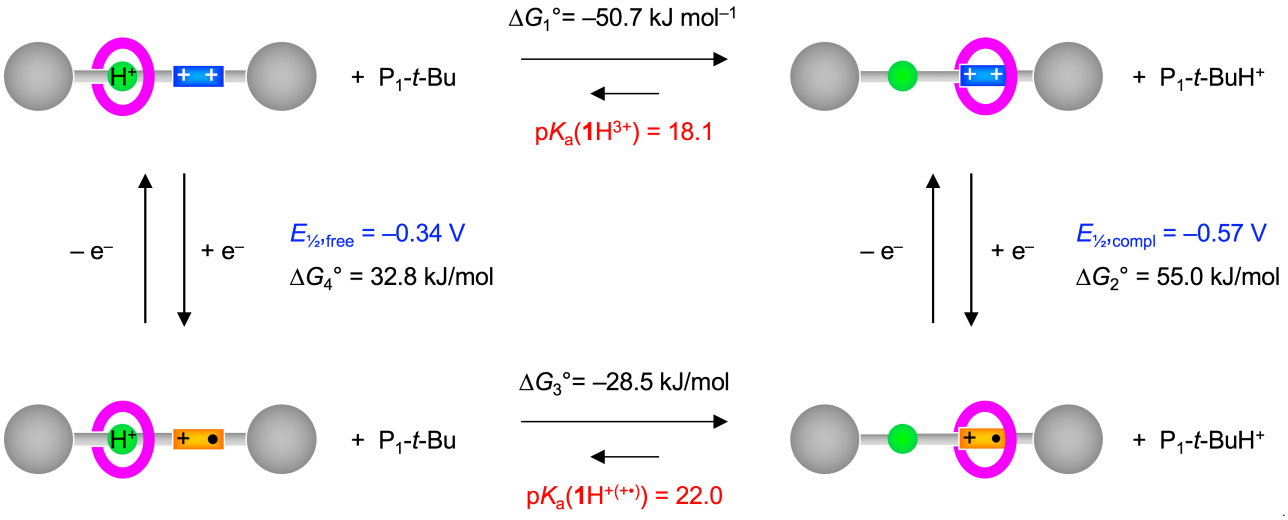

Fig. S12. Thermodynamic square cycle involving one-electron reduction/oxidation of the bpy^{2+} unit (vertical) and acid-base shuttling (horizontal) reactions. Data are referred to the reactions read from left to right and from top to bottom.

The difference between such ΔG° values ($\Delta G_2^\circ - \Delta G_4^\circ$) must be equal to the difference in the free energy change of the horizontal reactions of the cycle ($\Delta G_3^\circ - \Delta G_1^\circ$). The ring-axle interactions are the same in the starting states of both reactions (M⊃amH$^+$), whereas they are different in the final states (M⊃bpy^{2+} or M⊃bpy$^{(+\bullet)}$). Thus, the $\Delta(\Delta G^\circ)$ of these reactions quantifies the energy difference of charge-transfer interactions in the final states (equation S3), and corresponds to the energy difference $\beta - \alpha$ in Fig. S11C.

$$\Delta(\Delta G^\circ) = \Delta G_2^\circ - \Delta G_4^\circ = \Delta G_3^\circ - \Delta G_1^\circ = 22.2 \text{ kJ mol}^{-1} \qquad \text{(S3)}$$

From the data shown in Fig. S12 one can also calculate the pK_a value of the monoreduced rotaxane. In fact, ΔG_1° is related to the pK_a of P$_1$-*t*-BuH$^+$ and **1**H^{3+}, which are both known:

$$\Delta G_1^\circ = -\,2.303\,R\,T\,\text{Log}\,K_{eq} = -2.303\,R\,T\,\text{Log}[K_a(\mathbf{1}H^{3+})/K_a(P_1\text{-}t\text{-}BuH^+) =$$

$$= 2.303\ R\ T\ [pK_a(\mathbf{1}H^{3+}) - pK_a(P_1\text{-}t\text{-}BuH^+)] = -50.7\ \text{kJ mol}^{-1} \quad \text{(S4)}$$

The value of $\Delta G_3°$ can thus be calculated:

$$\Delta G_3° = \Delta G_1° + \Delta G_2° - \Delta G_4° = -28.5\ \text{kJ mol}^{-1} \quad \text{(S5)}$$

from which one can obtain the pK_a of the $\mathbf{1}H^{+(+\bullet)}$ rotaxane:

$$pK_a(\mathbf{1}H^{+(+\bullet)}) = pK_a(P_1\text{-}t\text{-}BuH^+) + \Delta G_3°/(2.303\ R\ T) = 22.0 \quad \text{(S6)}$$

A thermodynamic cycle similar to that of Fig. S12 but involving the $bpy^{(+\bullet)} \rightarrow bpy^{(0)}$ reduction can be devised (Fig. S13). From analogous considerations to those discussed above, one can calculate the $\Delta G°$ values of the processes and the pK_a of the $\mathbf{1}H^{+(0)}$ rotaxane (equations S7-S10).

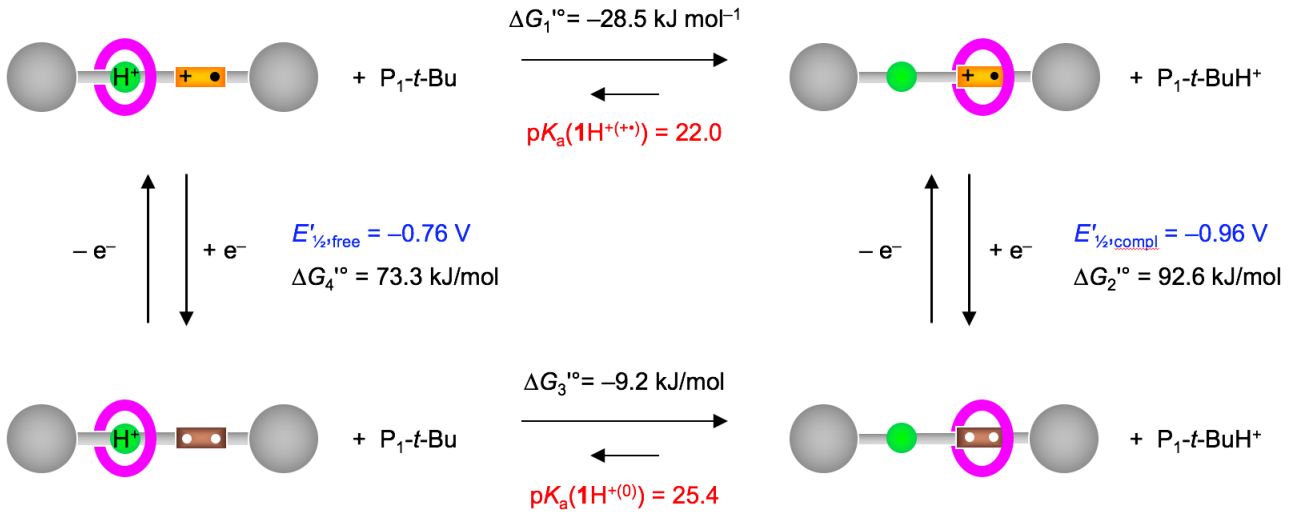

Fig. S13. Thermodynamic square cycle involving one-electron reduction/oxidation of the $bpy^{(+\bullet)}$ unit (vertical) and acid-base shuttling (horizontal) reactions. Data are referred to the reactions read from left to right and from top to bottom.

$$\Delta G_2'° = -z\ F\ E'°_{compl} \cong -z\ F\ E'_{½,compl} = -1 \times 96480 \times (-0.96) = 92.6\ \text{kJ mol}^{-1} \quad \text{(S7)}$$

$$\Delta G_4'° = -z\ F\ E'°_{free} \cong -z\ F\ E'_{½,free} = -1 \times 96480 \times (-0.76) = 73.3\ \text{kJ mol}^{-1} \quad \text{(S8)}$$

$$\Delta(\Delta G'°) = \Delta G_2'° - \Delta G_4'° = 19.3\ \text{kJ mol}^{-1} \quad \text{(S9)}$$

Note that $\Delta(\Delta G'°)$ corresponds to the energy difference $\gamma - \beta$ in Fig. S11C.

$$\Delta G_1'° = \Delta G_3° = -2.303\ R\ T\ \mathrm{Log}\ K_{eq} = -2.303\ R\ T\ \mathrm{Log}[K_a(\mathbf{1}H^{+(+\bullet)})/K_a(P_1\text{-}t\text{-}BuH^+) =$$
$$= 2.303\ R\ T\ [pK_a(\mathbf{1}H^{+(+\bullet)}) - pK_a(P_1\text{-}t\text{-}BuH^+)] = -28.5\ \mathrm{kJ\ mol^{-1}} \quad \text{(S10)}$$

$$\Delta G_3'° = \Delta G_1'° + \Delta G_2'° - \Delta G_4'° = -9.2\ \mathrm{kJ\ mol^{-1}} \quad \text{(S11)}$$

$$pK_a(\mathbf{1}H^{+(0)}) = pK_a(P_1\text{-}t\text{-}BuH^+) + \Delta G_3'°/(2.303\ R\ T) = 25.4 \quad \text{(S12)}$$

References

S1. Coetzee JF, Padmanabhan GR (1965) Properties of bases in acetonitrile as solvent. IV. Proton acceptor power and homoconjugation of mono- and diamines. *J Am Chem Soc* 87:5005-5010.

S2. Kaljurand I, Kütt A, Sooväli L, Rodima T, Mäemets V, Leito I, Koppel IA (2005) Extension of the self-consistent spectrophotometric basicity scale in acetonitrile to a full span of 28 pK_a units: Unification of different basicity scales. *J Org Chem* 70:1019-1028.